Complete-to-Overcomplete Discrete Wavelet Transforms: Theory and Applications

Yiannis Andreopoulos, *Student Member, IEEE*, Adrian Munteanu, Geert Van der Auwera, Jan P. H. Cornelis, *Member, IEEE*, and Peter Schelkens, *Member, IEEE*

***Abstract*—A new transform is proposed that derives the overcomplete discrete wavelet transform (ODWT) subbands from the critically sampled DWT subbands (complete representation). This complete-to-overcomplete DWT (CODWT) has certain advantages in comparison to the conventional approach that performs the inverse DWT to reconstruct the input signal, followed by the à-trous or the lowband shift algorithm. Specifically, the computation of the input signal is not required. As a result, the minimum number of downsampling operations is performed and the use of upsampling is avoided.**

The proposed CODWT computes the ODWT subbands by using a set of prediction-filter matrices and filtering-and-downsampling operators applied to the DWT. This formulation demonstrates a clear separation between the single-rate and multirate components of the transform. This can be especially significant when the CODWT is used in resource-constrained environments, such as resolution-scalable image and video codecs. To illustrate the applicability of the proposed transform in these emerging applications, a new scheme for the transform-calculation is proposed, and existing coding techniques that benefit from its usage are surveyed. The analysis of the proposed CODWT in terms of arithmetic complexity and delay reveals significant gains as compared with the conventional approach.

***Index Terms*—Complexity reduction, overcomplete discrete wavelet transforms, scalable image and video coding, shift invariance.**

I. Introduction

RECENTLY, wavelet-based image and video coding systems that utilize the overcomplete discrete wavelet transform (ODWT) have been proposed in the literature [1]–[16]. The good coding performance of these techniques stems from wavelet-domain operations that require shift-invariance, such as in-band motion estimation and compensation [1]–[9], in-band motion compensated temporal filtering [10]–[15], and phase-based prediction of wavelet coefficients [16]. The ODWT is used for this purpose since it is a redundant version of the discrete wavelet transform (DWT) that attains shift-invariance [19], [23].

Manuscript received May 7, 2003; revised February 26, 2004. This work was supported in part by the Federal Office for Scientific, Technical, and Cultural Affairs (IAP Phase V—Mobile Multimedia) and by the European Community under the IST Program (Mascot, IST-2000-26 467). Part of the work of P. Schelkens was supported by a post-doctoral fellowship with the Fund for Scientific Research—Flanders (FWO), Egmontstraat 5, B-1000 Brussels, Belgium. The associate editor coordinating the review of this manuscript and approving it for publication was Dr. Henrique Malvar.

The authors are with the Department of Electronics and Information Processing (ETRO), Vrije Universiteit Brussel, B-1050 Brussels, Belgium (e-mail: yandreop@etro.vub.ac.be; acmuntea@etro.vub.ac.be; gvdauwer@etro.vub.ac.be; jpcornel@etro.vub.ac.be; pschelke@etro.vub.ac.be).

Digital Object Identifier 10.1109/TSP.2005.843707

Given the input signal, the classical construction of the ODWT is trivial by using for example the "à-trous" algorithm [19], [23]. However, in wavelet-based coding systems, the codec always processes the critically sampled (complete) DWT subbands. Hence, a complete-to-overcomplete DWT (CODWT) has to take place: First, the inverse DWT is performed in order to reconstruct the input signal, followed by the ODWT [1], [2]. Furthermore, in many image and video-coding systems, the critically sampled DWT subbands may be processed in a *resolution-scalable* manner (from coarse to fine resolution) [4]–[16]. In such environments, it is imperative that both ends of the system *independently* construct the identical ODWT information at each resolution level in order to avoid drift effects [6], [7], [16]. Given the resolution levels that are available at both the encoder and decoder, a separate loop is used at each level for the CODWT in order to construct identical ODWT representations at both sides [5]–[9], [16]. This approach has several disadvantages.

- A direct method for the derivation of the ODWT subbands from the DWT is not provided. Instead, the ODWT construction is a cascade of the inverse DWT and the "à-trous" calculation. As a result, the reconstruction of the input signal is required. This causes significant calculation overhead and delay since the input signal has the highest sampling rate.
- A multirate calculation scheme is used in every case with a cascade of upsampling and downsampling operations. As a result, even for high-speed high-parallel implementations, the achievable percentage of hardware utilization is low since the filtering of every level has to be pipelined with the production of the results of the previous and the next level [24].

In this paper, we present a new theory for the CODWT, formulated for any arbitrary level k of the transform, in which the ODWT of level k is produced *directly* from the DWT of k-levels [4], [17]. The reconstruction of the input signal is not required, and furthermore, no upsampling is performed. Our initial findings reported in [4] and [17], as well as independent work reported recently by Li [18], present similar approaches for performing phase shifting in the wavelet domain. This paper generalizes these ideas to a transform that performs the direct construction of an *arbitrary* phase in the k-level wavelet domain (Proposition 2). In addition, we propose a direct solution for the (all-phase) CODWT (Proposition 3) and present an efficient calculation scheme for the transform. Apart from the new theoretical aspects arising from the proposed transform, we demonstrate the significant practical benefits of the new ap-

proach under the application scenarios that require resolution scalability. In such cases, the proposed CODWT is computed using a *single-rate* calculation scheme while providing exactly the same results as the conventional multi-rate approach.

The paper is structured as follows. Section II introduces the basic notations and definitions and presents the CODWT under different constraints. The CODWT formulation for the general case of level k is given in Section III. In addition, several properties of the proposed transform are discussed, and a novel scheme for the computation of the CODWT is presented. Section IV presents a complexity study that identifies the implementation benefits offered by the proposed transform. In order to demonstrate in more detail the applications that benefit from the proposed approach, some indicative results for scalable image and video coding based on CODWT are presented in Section V.

II. Problem Formulation

A. Notations and Symbolism

In this paper, bold-faced capital and lower letters indicate matrices and vectors, respectively, while $\mathbf{I}$ denotes the identity matrix. Calligraphic notation is reserved for operators (e.g., $\mathcal{D}$ denotes the polyphase separation). All signals and filters are considered in the Z-domain as Laurent polynomials, and the letter z is reserved for this purpose. All the used indices are integers. For all matrices, vectors, signals, and filters, the superscripts denote the decomposition level, except for superscript T, which denotes transposition. Subscripts are used to enumerate signals or filters in matrices and vectors. Additionally, they are used to indicate polyphase components; each case is identified from the context.

The polyphase separation of a signal or filter $X(z)$ is given by $\mathcal{D}X(z) = [X_0(z)\ X_1(z)]^T$, with the commutative operation given by $\mathcal{D}^{-1}\mathcal{D}X(z) = X_0(z^2) + zX_1(z^2) = X(z)$. For the DWT, the Type-I analysis polyphase matrices that produce the even and odd polyphase components of the transform are denoted as $E_0(z), E_1(z)$ respectively; their definitions are

$$\mathbf{E}_0(z) = \begin{bmatrix} H_0(z) & H_1(z) \\ G_0(z) & G_1(z) \end{bmatrix}, \quad \mathbf{E}_1(z) = \mathbf{E}_0(z) \begin{bmatrix} 0 & z \\ 1 & 0 \end{bmatrix}$$

where $H(z), G(z)$ are the lowpass and highpass analysis DWT filters, respectively. The corresponding Type-II synthesis polyphase matrices are $\mathbf{R}_i(z) = [\mathbf{E}_i(z)]^{-1}, i = \{0,1\}$, e.g.,

$$\mathbf{R}_0(z) = \frac{1}{\det \mathbf{E}_0(z)} \begin{bmatrix} G_1(z) & -H_1(z) \\ -G_0 & (z)H_0(z) \end{bmatrix}.$$

In order to simplify the expressions we always assume (without loss of generality) that the filters $H(z)$ and $G(z)$ are properly shifted so that perfect reconstruction is achieved with zero delay, and $\det \mathbf{E}_0(z) = -1$ [25, Sec. 3]. Using the Noble identity [25], the single-level filtering-and-downsampling operator can be written as $\mathcal{U}_i^1 = [\mathcal{D}(z^i U(z))]^T \mathcal{D}$, with $i = \{0,1\}$ denoting the retained polyphase component and $\mathcal{U} = \{\mathcal{H}, \mathcal{G}\}, U = \{H, G\}$, respectively. For l decomposition levels ($l \geq 1$), this operator is

$$\mathcal{U}_p^l = \mathcal{U}_{b_0}^1 \mathcal{H}_{b_1}^1 \ldots \mathcal{H}_{b_{l-1}}^1, \quad p = \sum_{i=0}^{l-1} b_i 2^i, \quad b_i = \{0,1\}. \quad (1)$$

Definition 1: For a signal $X(z)$ and an analysis filterbank $U = \{H, G\}$ with $\det \mathbf{E}_0(z) = -1$, we define $\mathbf{w}_p^l(z)$ as the p-phase wavelet subbands of the ODWT of decomposition level $E = l$ ($l \geq 1$) [5], [18], [23], given by $\mathbf{w}_p^l(z) = [A_p^l(z)\ D_p^l(z)]^T = [\mathcal{H}_p^l\ \mathcal{G}_p^l]^T X(z), 0 \leq p < 2^l$, where $A_p^l(z), D_p^l(z)$ are the low- and high-frequency subbands, respectively.

This definition coincides with the ODWT subbands calculated by the cycle-spinning algorithm of [26]: The binary representation of p is actually the binary map of the DWT defined in [26]. In total, the l-level ODWT of a signal $X(z)$ is given by $\boldsymbol{\mathcal{L}}_p^l X(z)$, for every $p, 0 \leq p < 2^l$, where

$$\boldsymbol{\mathcal{L}}_p^l = \begin{bmatrix} \boldsymbol{\lambda}_{p,\mathcal{H}}^l \\ \boldsymbol{\lambda}_{p,\mathcal{G}}^l \end{bmatrix}$$

is a $2 \times l$ matrix operator, and $\boldsymbol{\lambda}_{p,\mathcal{U}}^l = [\mathcal{U}_{b_0}^1\ \mathcal{U}_{b_0+2b_1}^2 \cdots \mathcal{U}_p^l]$. For example, for $l = 1$, we have $\boldsymbol{\mathcal{L}}_p^1 = \mathbf{E}_p(z)\mathcal{D}, p = \{0,1\}$. The following lemma establishes the $\boldsymbol{\mathcal{L}}_p^l$ operator recursively.

Lemma 1: The $\boldsymbol{\mathcal{L}}_p^l$ operator applied on signals $\mathbf{x}(z) = [X_{l-1}(z) \cdots X_0(z)]^T$ and $X_l(z)$, with $X_q(z), 0 \leq q \leq l$, having a sampling rate of 2^{-q}, satisfies

$$\boldsymbol{\mathcal{L}}_i^1 \left(X_l(z) + \boldsymbol{\lambda}_{p,\mathcal{H}}^l \mathbf{x}(z) \right) = \boldsymbol{\mathcal{L}}_{2p+i}^{l+1} \begin{bmatrix} X_l(z) \\ \mathbf{x}(z) \end{bmatrix}, \quad i = \{0,1\}. \quad (2)$$

Proof: By expanding the right part of (2) using (1) and the definition of the $\boldsymbol{\mathcal{L}}_p^l$ operator, we reach the left part as follows:

$$\begin{aligned} \boldsymbol{\mathcal{L}}_{2p+i}^{l+1} \begin{bmatrix} X_l(z) \\ \boldsymbol{x}(z) \end{bmatrix} &= \begin{bmatrix} \mathcal{H}_i^1 & \mathcal{H}_{i+2b_0}^2 & \cdots & \mathcal{H}_{2p+i}^{l+1} \\ \mathcal{G}_i^1 & \mathcal{G}_{i+2b_0}^2 & \cdots & \mathcal{G}_{2p+i}^{l+1} \end{bmatrix} \begin{bmatrix} X_l(z) \\ \mathbf{x}(z) \end{bmatrix} \\ &= \begin{bmatrix} \mathcal{H}_i^1 \\ \mathcal{G}_i^1 \end{bmatrix} X_l(z) + \begin{bmatrix} \mathcal{H}_i^1 \\ \mathcal{G}_i^1 \end{bmatrix} \boldsymbol{\lambda}_{p,\mathcal{H}}^l \mathbf{x}(z). \end{aligned} \quad (3)$$

■

B. Problem Description

In this section, we briefly present two methods for the CODWT under the image and video coding scenarios of interest [1]–[16]. The first method is based on the IDWT followed by the lowband shift (LBS) method [1], [23]. The LBS can be seen as a specific implementation technique of the "à-trous" algorithm [19], where the different ODWT subbands are produced and stored according to the retained polyphase components. The second method represents our proposed approach.

Fig. 1(a) shows an example of the 1-D ODWT for three decomposition levels starting from an input signal $X(z)$. This figure facilitates the description of the LBS method [1], [2], [23]. Initially, the input signal $X(z)$ is decomposed in two subband sets $A_0^1(z), D_0^1(z)$ and $A_1^1(z), D_1^1(z)$ by retaining separately the

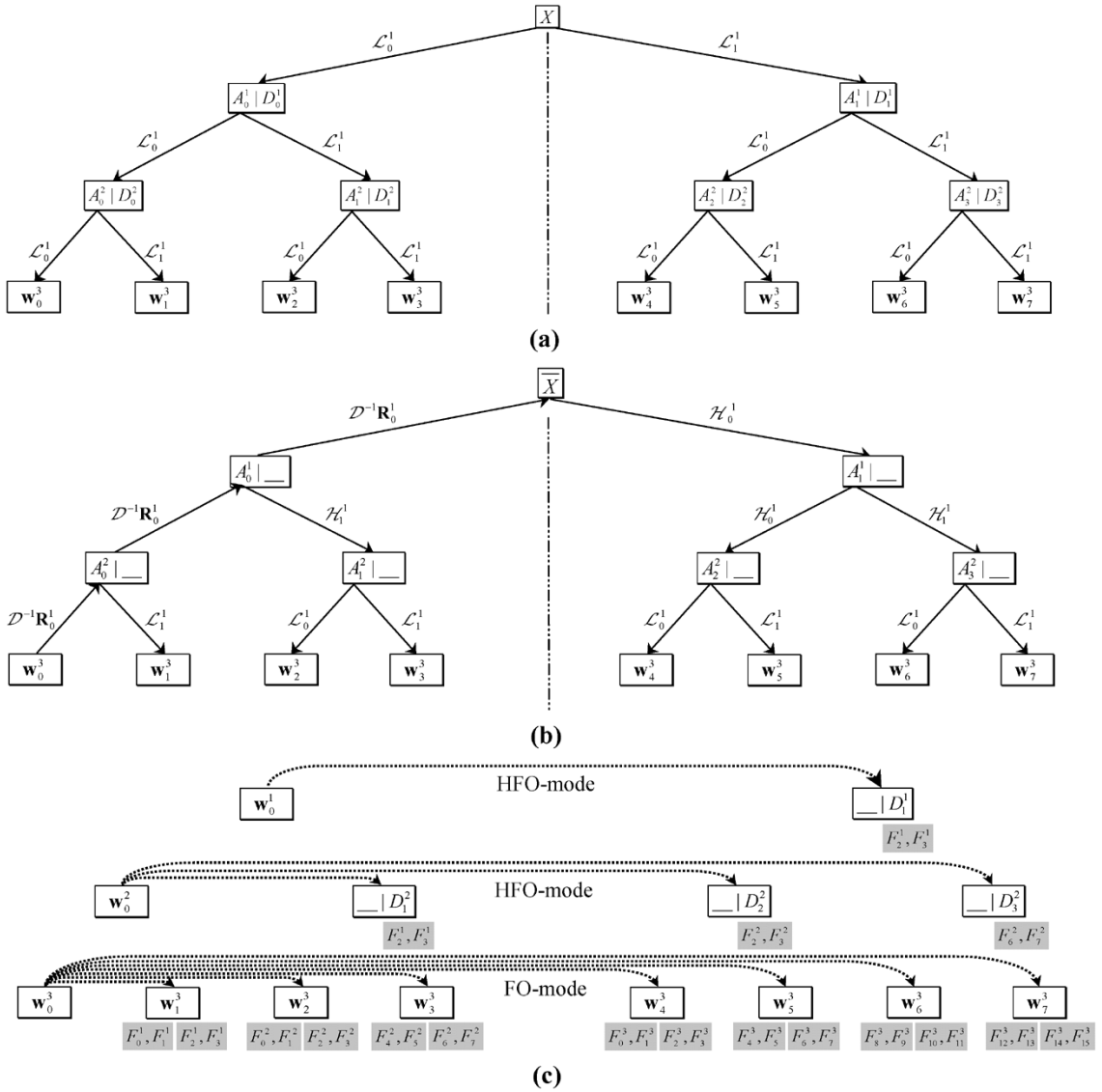

Fig. 1. (a) Construction of the ODWT of three levels starting from the input signal X. A number of one-level discrete wavelet transforms are performed that retain the even or odd samples of the nondecimated transform ($\mathcal{L}_i^1$ with $i = 0, 1$, respectively). (b) Level-by-level construction of the ODWT (example for level 3) using the conventional multirate IDWT and LBS approach that perform a set of inverse and forward transforms. (c) Level-by-level construction of the ODWT for all three levels using the proposed single-rate approach.

even and odd polyphase components of the nondecimated decomposition, respectively, or, equivalently, by performing two wavelet decompositions: one to the zero-shifted and one to the unit-shifted input signal, respectively [1], [2], [23]. Each of the low-frequency subbands $A_0^1(z)$ and $A_1^1(z)$ is further analyzed in the same manner, while the high-frequency subbands $D_0^1(z)$ and $D_1^1(z)$ are the outputs of the first decomposition level. This process is repeated successively, yielding the ODWT representation from the input signal $X(z)$ [see Fig. 1(a)] [1], [23]. The subbands $A_0^3(z)$ and $D_0^l(z), l = 1, 2, 3$ represent the critically sampled (complete) DWT of three decomposition levels, while the subbands $A_i^3(z), D_i^l(z), 1 \leq l \leq 3, 1 \leq i < 2^l$ represent the calculated ODWT. Hence, for the CODWT based on this method, the signal $X(z)$ has to be reconstructed by performing the IDWT to the subbands $A_0^3(z), D_0^l(z)$, followed by the LBS.

Notice that the subbands $A_i^3(z), D_i^l(z)$ shown in Fig. 1(a) stem from the classical ODWT decomposition scheme of [23], which is equivalent to the "à-trous" algorithm [19]. The difference is that, at every level, the subbands of Fig. 1(a) must be interleaved in order to produce the nondecimated ODWT obtained with the algorithm of [23]. As a result, any subband $D_i^l(z)$ in the ODWT of Fig. 1(a) is the ith polyphase component of the nondecimated ODWT of level l [23], [19].

In the two-dimensional (2-D) case, the 2-D ODWT can be constructed in the same manner as in Fig. 1(a), by applying the LBS method on the input-subband rows and on the columns of the results [1], [23]. Hence, to facilitate the description, we focus in the following analysis on the 1-D case, with the extension in 2-D following the row-column approach.

In a progressive resolution-refinement (resolution scalable) framework, the additional constraint that the subband coding and decoding occurs in a bottom-up manner is imposed [4]–[16]: The coarsest-resolution subbands of the DWT are processed independently (subbands $A_0^3(z), D_0^3(z)$) and for every higher resolution level l with $l = 2, 1$, the subband $D_0^l(z)$ is additionally processed. In the case of hybrid (closed-loop) systems, these subbands are decoded at predefined base-quality levels. In this way, for each target resolution-level $l = 3, 2, 1,$

the encoder uses the same reference frames as the decoder will be able to create at the client side, and no drift occurs across resolutions [5]–[9]. This can be seen as an extension of the base-layer concept used in quality-progressive closed-loop video coding [27]; although the creation of the reference frames at the base-layer potentially lowers the performance of the subset of decoders that progressively process additional quality layers (or resolution levels in our case), this guarantees drift-free operation [5], [7], [9], [27].

Under such a resolution-scalable coding framework, the CODWT based on the LBS method is readily adaptable to perform a *level-by-level* construction of the ODWT representation (denoted by LL-LBS), starting from the subbands of the critically sampled transform of each decoded level. This process is illustrated in Fig. 1(b). Starting from the DWT subbands $\mathbf{w}_0^3(z)$ (coarsest resolution level), three single-level inverse wavelet transforms are performed. Subsequently, from the reconstructed signal $(\bar{X}(z))$, all the subbands $\mathbf{w}_i^3(z), 1 \leq i < 8$ are constructed by performing the single-level forward transforms shown in Fig. 1(b). It is important to notice that, since in this case the subbands $D_0^2(z), D_0^1(z)$ are not available, the reconstructed signal $\bar{X}(z)$ and the subbands $\mathbf{w}_i^3(z)$ are only an approximation of $X(z)$ and of the original ODWT of level 3, respectively, shown in Fig. 1(a). However, in this resolution-scalable scenario, given the common information available at both the encoder and decoder sides, this ODWT representation is the best possible approximation for the current resolution level [4]–[16]. Finally, if higher resolution versions of the input data are required, the ODWT construction by the LL-LBS is repeated for the finer resolution levels ($l = 2$ or $l = 1$, depending on the target resolution) [5]–[16].

Notice that in coding applications, for every decomposition level l, the low-frequency subbands $A_j^l(z), 1 \leq j < 2^l$ are part of the calculated ODWT only if level l is the coarsest resolution of the decomposition, i.e., if $l = 3$ in the example of Fig. 1(c) [5], [7], [11], [17]. We define this construction that generates the signals

$$\mathbf{w}_{\mathrm{ODWT}}^l(z) = \begin{bmatrix} \mathbf{w}_1^l(z) \\ \vdots \\ \mathbf{w}_{2^l-1}^l(z) \end{bmatrix}$$

as the *full-overcomplete* transform-production mode (FO-mode). In all the other cases [levels $l = 2, 1$ of Fig. 1(c)], the critically sampled DWT consists of the subband $D_0^l(z)$, and hence, in coding applications, only the high-frequency ODWT subbands $D_1^l(z), \ldots, D_{2^l-1}^l(z)$ need to be calculated [5]–[16]; this case is defined as the *high-frequency overcomplete* transform-production mode (HFO-mode). The difference between the FO and HFO modes is illustrated in Fig. 1(c).

Additionally, Fig. 1(c) presents the proposed alternative approach to the LL-LBS method for the level-by-level CODWT of levels 3, 2, and 1. In this approach, the CODWT uses a set of prediction filters [4], [17], which are denoted as $F_j^i(z), 1 \leq i \leq 3, 0 \leq j < 2^{i+1}$ and are convolved with the subbands $A_0^i(z), D_0^i(z)$ to calculate the ODWT representation of each level. Notice that for levels 2 and 1 of Fig. 1(c), the ODWT construction occurs in the HFO mode, i.e., only the high-frequency subbands of the ODWT are calculated. Additionally, the figure illustrates that by using the prediction-filters, the overcomplete representation of each level is "predicted," as shown with the dotted lines. As a result, no upsampling is performed, and no reconstruction of the spatial-domain signal $X(z)$ is required. The mathematical derivation of the prediction filters and the proposed CODWT are presented next.

III. Complete to Overcomplete Representations

In this section, we present a generic framework for the calculation of the ODWT subbands of decomposition level k as a function of the critically sampled wavelet decomposition (i.e., the subbands $A_0^k(z), D_0^l(z)$, with $1 \leq l \leq k$). From this formalism, the level-by-level CODWT of level k, which is especially interesting for applications requiring progressive-refinement in resolution (e.g., [5]–[16]), can be found as a special case. A symmetry property for the prediction filters of every level is also proven. Based on this property, an efficient scheme for the CODWT calculation is presented.

A. Derivation of the ODWT Subbands of Decomposition Level k From the k-Level DWT—The Prediction Filters

We start with by exemplifying the proposed CODWT for levels $E = 1, 2$ (Section III-A1). Then, Section III-A2 formulates the CODWT for any arbitrary level $E = k$.

1) Calculation of the ODWT Subbands of Levels $E = 1$ and $E = 2$:

Definition 2: We define $\mathbf{F}_0^1(z)$ and $\mathbf{F}_i^2(z), i = \{0, 1\}$ as the prediction-filter matrices of levels $E = 1$ and $E = 2$, respectively. They are given by (4) and (5), shown at the bottom of the page, where $F_{0,i}^1(z)$ and $F_{0,1-i}^1(z)$ are the i and $1-i$ polyphase components of filter $F_0^1(z)$, respectively.

Proposition 1: The subbands $\mathbf{w}_1^1(z)$ of the ODWT of level $E = 1$ are given by

$$\mathbf{w}_1^1(z) = \mathbf{F}_0^1(z)\mathbf{w}_0^1(z) \tag{6}$$

while subbands $\mathbf{w}_1^2(z), \mathbf{w}_2^2(z), \mathbf{w}_3^2(z)$ of the ODWT of level $E = 2$ are

$$\begin{aligned} \mathbf{w}_1^2(z) &= \mathbf{F}_0^1(z)\mathbf{w}_0^2(z) \\ \mathbf{w}_{2+i}^2(z) &= \mathbf{F}_i^2(z)\mathbf{w}_0^2(z) + \boldsymbol{\mathcal{L}}_i^1\left(F_1^1(z)D_0^1(z)\right), \quad i = \{0, 1\}. \end{aligned} \tag{7}$$

$$\mathbf{F}_0^1(z) = \begin{bmatrix} F_0^1(z) & F_1^1(z) \\ F_2^1(z) & F_3^1(z) \end{bmatrix} = \begin{bmatrix} zH_0(z)G_0(z) - H_1(z)G_1(z) & H_1(z)H_1(z) - zH_0(z)H_0(z) \\ zG_0(z)G_0(z) - G_1(z)G_1(z) & H_1(z)G_1(z) - zH_0(z)G_0(z) \end{bmatrix} \tag{4}$$

$$\mathbf{F}_i^2(z) = F_{0,i}^1(z)\mathbf{I} + z^{-(1-i)}F_{0,1-i}^1(z)\mathbf{F}_0^1(z) \tag{5}$$

Proof: The proof of (6) can be derived by performing an inverse transform to subbands $\mathbf{w}_0^1(z)$ followed by a forward wavelet transform that retains the odd polyphase components of the nondecimated decomposition, as shown in Fig. 1(a). In total

$$\mathbf{w}_1^1(z) = \mathbf{E}_1(z)\mathcal{D}\mathcal{D}^{-1}\mathbf{R}_0(z)\mathbf{w}_0^1(z) = \mathbf{F}_0^1(z)\mathbf{w}_0^1(z)$$

where $\mathbf{F}_0^1(z)$ is the prediction-filter matrix given in (4).

Applying an inverse wavelet transform to subbands $\mathbf{w}_0^2(z)$ yields $A_0^1(z) = \mathcal{D}^{-1}(\mathbf{R}_0(z)\mathbf{w}_0^2(z))$. Then, as shown in Fig. 1(a), by performing a forward transform that retains the odd polyphase components of the nondecimated transform, we reach the subbands $\mathbf{w}_1^2(z)$ given in (7). Additionally, by using a part of (6), we derive the subband $A_1^1(z)$ as $A_1^1(z) = [F_0^1(z)\ F_1^1(z)]\mathbf{w}_0^1(z)$. The final result is reached by performing a forward wavelet transform retaining the even or odd polyphase components for $i = 0, 1$, respectively, and using the Noble identity that exchanges the filtering and downsampling order [25]. Hence

$$\begin{aligned}\mathbf{w}_{2+i}^2(z) &= \mathbf{E}_i(z)\mathcal{D}A_1^1(z)\\ &= \mathbf{E}_i(z)\left(F_{0,0}^1(z)\mathbf{I} + z^{-1}F_{0,1}^1(z)\begin{bmatrix}0 & z\\ 1 & 0\end{bmatrix}\right)\\ &\quad\times \mathbf{R}_0(z)\mathbf{w}_0^2(z) + \boldsymbol{\mathcal{L}}_i^1\left(F_1^1(z)D_0^1(z)\right)\\ &= \mathbf{F}_i^2(z)\mathbf{w}_0^2(z) + \boldsymbol{\mathcal{L}}_i^1\left(F_1^1(z)D_0^1(z)\right)\end{aligned} \tag{8}$$

where $\mathbf{F}_i^2(z)$ is the prediction-filter matrices given in (5). ■

Proposition 1 hints that in the general case of an arbitrary level $k, k > 1$, the calculation of the ODWT subbands from the k-level DWT involves a) the single-rate filtering of the DWT subbands of level k ($\mathbf{w}_0^k(z)$) and b) the cascade application of filtering-and-downsampling operations to the high-frequency subbands of higher-resolution levels of the DWT $(D_0^{k-1}(z), \ldots, D_0^1(z))$. This intuitive link is mathematically formulated next.

2) Calculation of the ODWT Subbands of Level $E = k$: The generalization of Proposition 1 and the corresponding definitions are given below for an arbitrary level $E = k$.

Definition 3: We define $\mathbf{F}_p^{l+1}(z)$ as the prediction- filter matrices of level $E = l+1, 1 \le l < k$ with $k > 1$, given by

$$\begin{aligned}\mathbf{F}_p^{l+1}(z) &= \begin{bmatrix}F_{4p}^{l+1}(z) & F_{4p+1}^{l+1}(z)\\ F_{4p+2}^{l+1}(z) & F_{4p+3}^{l+1}(z)\end{bmatrix}\\ &= F_{w(1),b_0}^l(z)\mathbf{I} + z^{-(1-b_0)}F_{w(1),1-b_0}^l(z)\mathbf{F}_0^1(z)\end{aligned} \tag{9}$$

where $F_{w(1)}^l(z)$ are prediction filters of level $E = l$, the filter subscripts $w(m)$ are defined as $w(m) = 4\lfloor(p/2^m)\rfloor, 1 \le m \le l$, and p given by (1).

Definition 4: We define $\mathbf{F}_d^l(z)$ as the diagonal matrix of prediction filters given by

$$\mathbf{F}_d^l(z) = \operatorname{diag}\left(F_{w(1)+1}^l(z) \quad F_{w(2)+1}^{l-1}(z) \quad \cdots \quad F_{w(l)+1}^1(z)\right).$$

Definition 5: We define $\mathbf{d}^{k-1,l}(z), 1 \le l < k$ with $k > 1$ as the vector of high-frequency subbands of levels $k-1, k-2, \ldots, k-l$ of the DWT. It is given by

$$\mathbf{d}^{k-1,l}(z) = \begin{bmatrix}D_0^{k-1}(z) & D_0^{k-2}(z) & \cdots & D_0^{k-l}(z)\end{bmatrix}^T.$$

Proposition 2: The subbands of the ODWT of level $E = k, \mathbf{w}_x^k(z)$, with $1 \le x < 2^k$, are given by

$$\mathbf{w}_x^k(z) = \mathbf{F}_p^{l+1}(z)\mathbf{w}_0^k(z) + \boldsymbol{\mathcal{L}}_p^l\left(\mathbf{F}_d^l(z)\mathbf{d}^{k-1,l}(z)\right) \tag{10}$$

where x denotes the ODWT-subband index at level k (phase x) and is written as $x = 2^l + p$, while l, p are given as in Definition 3, and $l = \lfloor \log_2 x \rfloor$. In the particular case of $l = 0$ corresponding to $k = 1$ and $x = 1$, we set $p = 0$ and $\boldsymbol{\mathcal{L}}_0^0 \equiv [0\ 0]^T$ (zero operator) as well as $F_A^B(z) \equiv 0$ for any indices $A < 0$ or $B \le 0$. For this case, (10) becomes Proposition 1.

Proof: The proof is inductive. Initially, it is noted that (10) holds for levels $E = 1$ and $E = 2$ since it corresponds to Proposition 1. Subsequently, assume that (10) holds for a particular $E = k$. It is now proven that, given the subbands $\mathbf{w}_0^{k+1}(z)$ (DWT subbands of level $k+1$), if (10) holds for $E = k$, it holds also for $E = k+1$.

Let us start by performing an inverse DWT in order to calculate the A_0^k subband in function of subbands $\mathbf{w}_0^{k+1}(z)$:

$$A_0^k(z) = \mathcal{D}^{-1}\left(\mathbf{R}_0(z)\mathbf{w}_0^{k+1}(z)\right). \tag{11}$$

The derivation of subbands $\mathbf{w}_1^{k+1}(z)$ follows immediately by performing a forward transform with $\mathbf{E}_1(z)$. Hence, we derive (10) for the special case of $x = 1$ with k replaced by $k+1$. For the remaining subbands of level $k+1$, we can apply (10) (involving the filters of the $\mathbf{F}_p^{l+1}(z)$ matrix) since it is true for level $E = k$. We can calculate any subband $A_x^k, 1 < x < 2^k$ as

$$\begin{aligned}A_x^k(z) = \begin{bmatrix}F_{4p}^{l+1}(z) & F_{4p+1}^{l+1}(z)\end{bmatrix}\mathbf{w}_0^k(z)\\ + \boldsymbol{\lambda}_{p,\mathcal{H}}^l\left(\mathbf{F}_d^l(z)\mathbf{d}^{k-1,l}(z)\right).\end{aligned} \tag{12}$$

As shown in Fig. 1(b) for the example of $k = 2$, in order to calculate the $\mathbf{w}_{2x}^{k+1}(z)$ subbands (even-numbered subbands of level $k+1$), we need to perform a single-level forward transform in (12), retaining the even samples ("classical" DWT):

$$\begin{aligned}&\mathbf{w}_{2x}^{k+1}(z) = \mathbf{E}_0(z)\mathcal{D}\left(F_{4p}^{l+1}(z)A_0^k(z)\right)\\ &+ \mathbf{E}_0(z)\mathcal{D}\left[F_{4p+1}^{l+1}(z)D_0^k(z) + \boldsymbol{\lambda}_{p,\mathcal{H}}^l\left(\mathbf{F}_d^l(z)\mathbf{d}^{k-1,l}(z)\right)\right].\end{aligned} \tag{13}$$

Based on Lemma 1, (11), and the Noble identity, the last equation can be written as

$$\begin{aligned}\mathbf{w}_{2x}^{k+1}(z) &= \mathbf{E}_0(z)\left(F_{4p,0}^{l+1}(z)\mathbf{I} + z^{-1}F_{4p,1}^{l+1}(z)\begin{bmatrix}0 & z\\ 1 & 0\end{bmatrix}\right)\\ &\quad\times \mathbf{R}_0(z)\mathbf{w}_0^{k+1}(z) + \boldsymbol{\mathcal{L}}_{2p}^{l+1}\left(\mathbf{F}_d^{l+1}(z)\mathbf{d}^{k,l+1}(z)\right).\end{aligned} \tag{14}$$

After simplifications, (14) becomes equivalent to (10) with l replaced by $l' = l+1$ and, hence, $2 \le l' < k+1$, while the ODWT subband index $2x$ of (14) is bounded by $2 \le 2x < 2^{k+1}$. In addition, the resulting prediction- filter matrix of (14) is expressed as in (9) with $p' = \sum_{i=1}^{l'-1} c_i 2^i$ and $c_i = b_{i-1}, c_0 = 0$. Hence,

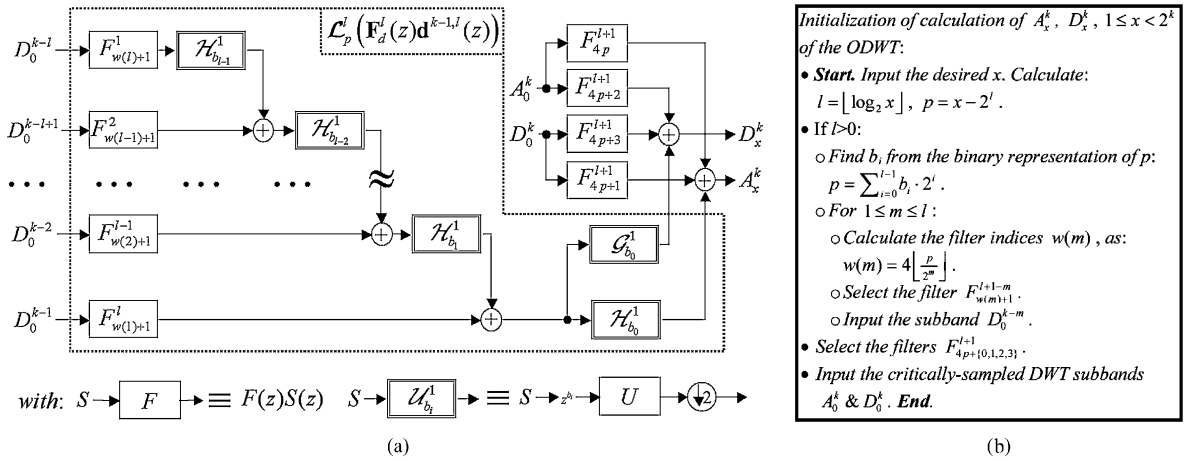

Fig. 2. (a) Straightforward calculation of the CODWT based on Proposition 2. (b) Initialization of the calculation of A_x^k, D_x^k.

(14) corresponds to (10) for the even-numbered subbands, with k replaced by $k+1$.

In order to calculate the subbands $\mathbf{w}_{2x+1}^{k+1}(z)$ (odd-numbered subbands of level $k+1$), we perform a forward DWT retaining the odd samples, reaching, similarly as before, the following:

$$\mathbf{w}_{2x+1}^{k+1}(z) = \mathbf{E}_1(z)\left(F_{4p,0}^{l+1}(z)\mathbf{I} + z^{-1}F_{4p,1}^{l+1}(z)\begin{bmatrix}0 & z\\ 1 & 0\end{bmatrix}\right) \times \mathbf{R}_0(z)\mathbf{w}_0^{k+1}(z) + \boldsymbol{\mathcal{L}}_{2p+1}^{l+1}\left(\mathbf{F}_d^{l+1}(z)\mathbf{d}^{k,l+1}(z)\right). \quad (15)$$

After simplifications, (15) becomes (10) with l replaced by $l' = l+1$ and, hence, $2 \le l' < k+1$, while the ODWT subband index $2x+1$ of (15) is bounded by $3 \le 2x+1 < 2^{k+1}$. In addition, the resulting prediction-filter matrix of (15) is expressed as in (9) with $p' = \sum_{i=1}^{l'-1} c_i 2^i$ and $c_i = b_{i-1}, c_0 = 1$. As a result, (15) corresponds to (10) for the odd-numbered subbands, with k replaced by $k+1$. One concludes that Proposition 2 is true for the case of $E = k+1$. This means, by induction, that it is true for every $E, E \ge 1$. ■

For each decomposition level k of the DWT, Proposition 2 given in (10) consists of a *single-rate* and a *multirate* calculation part. The first consists of the convolution of the critically sampled subbands of level k with the prediction filters of the matrix $\mathbf{F}_p^{l+1}(z), 0 \le l < k$, while the second consists of the convolutions of the vector of high-frequency DWT subbands of levels $k-1, k-2, \ldots, k-l$ with the diagonal matrix of prediction filters, followed by the successive filtering-and-downsampling with the analysis filters. This result is summarized below.

Proposition 3: The complete-to-overcomplete discrete wavelet transform of any level k is

$$\mathbf{w}_{\mathrm{ODWT}}^k(z) = \begin{bmatrix}\mathbf{P}^1(z)\\ \mathbf{P}^2(z)\\ \vdots\\ \mathbf{P}^k(z)\end{bmatrix}\mathbf{w}_0^k(z) + \begin{bmatrix}\boldsymbol{\mathcal{Q}}^0\\ \boldsymbol{\mathcal{Q}}^1\\ \vdots\\ \boldsymbol{\mathcal{Q}}^{k-1}\end{bmatrix}\left(\mathbf{F}_d^{k-1}(z)\mathbf{d}^{k-1,k-1}(z)\right) \quad (16)$$

with

$$\mathbf{w}_{\mathrm{ODWT}}^k(z) = \begin{bmatrix}\mathbf{w}_1^k(z)\\ \vdots\\ \mathbf{w}_{2^k-1}^k(z)\end{bmatrix}, \quad \mathbf{P}^{l+1}(z) = \begin{bmatrix}\mathbf{F}_0^{l+1}(z)\\ \mathbf{F}_1^{l+1}(z)\\ \vdots\\ \mathbf{F}_{2^l-1}^{l+1}(z)\end{bmatrix}$$

$$\boldsymbol{\mathcal{Q}}^l = \begin{bmatrix}\boldsymbol{\mathcal{L}}_0^l & 0 & \cdots & 0\\ \boldsymbol{\mathcal{L}}_1^l & 0 & \cdots & 0\\ \vdots & \vdots & \ddots & \vdots\\ \boldsymbol{\mathcal{L}}_{2^l-1}^l & & \cdots & 0\end{bmatrix} \mathbf{a}\ 2^{l+1} \times (k-1)$$

array of operators for every $0 \le l < k$, and $\boldsymbol{\mathcal{Q}}^0 = \boldsymbol{\mathcal{L}}_0^0 = \begin{bmatrix}0\\ 0\end{bmatrix}$.

B. Properties of the Derived Formulation

A straightforward calculation of any given subband pair $\mathbf{w}_x^k(z)$ of Proposition 2 is given schematically in Fig. 2, which also gives a pseudo-program describing the initialization procedure used to select the appropriate filters involved in the calculation of an arbitrary set of ODWT subbands $\mathbf{w}_x^k(z)$ of (10). The calculation of the multirate part of (10) shown in Fig. 2 is based on the following derivation:

$$\begin{aligned}&\boldsymbol{\mathcal{L}}_p^l\left(\mathbf{F}_d^l(z)\mathbf{d}^{k-1,l}(z)\right)\\ &\quad= \begin{bmatrix}\mathcal{H}_{b_0}^1\\ \mathcal{G}_{b_0}^1\end{bmatrix}\left(F_{w(1)+1}^l(z)D_0^{k-1}(z)\right.\\ &\quad+ \mathcal{H}_{b_1}^1\left(F_{w(2)+1}^{l-1}(z)D_0^{k-2}(z)\right.\\ &\quad+ \left.\left.\mathcal{H}_{b_2}^1\left(\cdots + \mathcal{H}_{b_{l-1}}^1\left(F_{w(l)+1}^1(z)D_0^{k-l}(z)\right)\cdots\right)\right)\right)\end{aligned} \quad (17)$$

which comes from the property that the downsampling and summation operations can be interchanged. Fig. 2 shows that the proposed approach involves the minimum number of downsampling operations and no upsampling is used.

In the following parts of this section, we present a symmetry property for the prediction filters of each decomposition level as well as an efficient calculation scheme of the single-rate and multirate parts of Proposition 3.

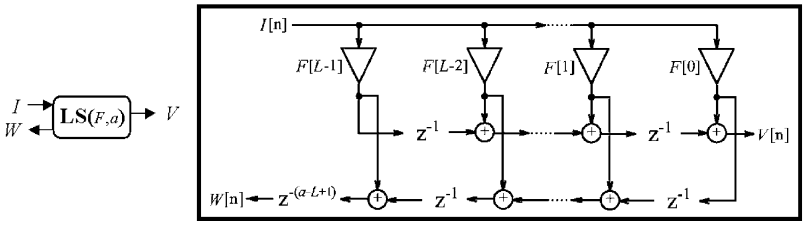

Fig. 3. Lattice structure that implements the two convolutions $V(z) = F(z)I(z)$ and $W(z) = z^{-a}F(z-1)I(z)$ for a filter F with L taps using L multipliers.

1) Symmetry Properties of the $F^l_{w(1)}$ Filters: Equation (9) provides some insight for the reduction of the necessary operations for the production of all the different subbands $\boldsymbol{w}^k_x(z)$. Below, we demonstrate a useful symmetry property.

Proposition 4: For the prediction-filter matrices $\mathbf{F}^{l+1}_p(z)$ of any level $E = l+1, 1 \le l < k$, the following property holds:

$$F^l_{w(1)}(z) = zF^l_{2^{l+1}-4-w(1)}(z^{-1}) \tag{18}$$

with $0 \le p < 2^{l-1}$ and $w(1)$ defined as for (9).

Proof: The proof is inductive. Hence, for $E = 1$

$$F^1_0(z) = zF^1_0(z^{-1}). \tag{19}$$

In Definition 1, we have assumed zero-delay perfect reconstruction with $\det \mathbf{E}_0(z) = -1$, which can be satisfied with $G(z) = G(z^{-1}), H(z) = z^{-2}H(z^{-1})$ for biorthogonal point-symmetric filter-pairs, $G(z) = -z^{-1}G(z^{-1}), H(z) = z^{-1}H(z^{-1})$ for biorthogonal half-point symmetric filter pairs, and $G(z) = z^{-1}H(-z^{-1})$ for orthogonal filter pairs. Based on these equations, the proof of (19) is concluded for each case by deriving the symmetry relations between the Type-I polyphase components of the analysis filters and using them in combination with the definition of $F^1_0(z)$ of (4).

Assuming that the proposition of (18) is true for the case of level $E = l$, in the Type-I polyphase components of $F^l_{w(1)}(z)$, we can replace the terms $F^l_{w(1)}(z^{1/2}), F^l_{w(1)}(-z^{1/2})$ by (18), yielding

$$\begin{aligned} F^l_{w(1),0}(z) &= zF^l_{2^{l+1}-4-w(1),1}(z^{-1}) \\ F^l_{w(1),1}(z) &= zF^l_{2^{l+1}-4-w(1),0}(z^{-1}) \end{aligned} \tag{20}$$

where $0 \le p < 2^{l-1}$. If we further impose that p is even, then we have $b_0 = 0$ according to the definition of p in (1). Combining the general definition of the prediction filters of (9) (which is true for level $l+1$) and (19) and (20), we reach, after several manipulations, (18), where l is replaced by $l+1$. If we impose that p is odd, the equivalent result is reached in the same manner. We conclude that the proposition of (18) is true for every level l, where $0 \le p < 2^{l-1}$. ■

A corollary of Proposition 4 is that (20) holds as well.

2) Calculation of the Single-Rate Part of the Proposed CODWT: Based on the derived symmetry property of (20), having the same input signal, the convolutions with filters $F^l_{w(1),0}(z), F^l_{w(1),1}(z)$ can be reused to produce the convolutions with the filters $F^l_{2^{l+1}-4-w(1),1}(z), F^l_{2^{l+1}-4-w(1),0}(z)$, respectively. This is achieved by using a lattice structure (LS) such as the one depicted in Fig. 3. This is of great practical importance since the utilization of this symmetry in the prediction filters of (9) leads to the reduction of the necessary arithmetic operations for the proposed CODWT. As an example, based on (20), if we expand the form of the prediction filters of (9) in the general expression of (16) for $k = 3$, with the setting $\mathbf{d}^{2,2}_0(z) = \mathbf{0}$ (single-rate calculation), we reach the following result:

$$\begin{aligned} &\mathbf{w}^3_1(z) = \mathbf{F}^1_0(z)\mathbf{w}^3_0(z) \\ &\begin{bmatrix}\mathbf{w}^3_2(z) & \mathbf{w}^3_3(z)\end{bmatrix} \\ &\quad = \begin{bmatrix}\mathbf{w}^3_0(z) & \mathbf{w}^3_1(z)\end{bmatrix} \begin{bmatrix} F^1_{0,0}(z) & zF^1_{0,0}(z^{-1}) \\ F^1_{0,0}(z^{-1}) & F^1_{0,0}(z)\end{bmatrix} \\ &\begin{bmatrix}\mathbf{w}^3_4(z) & \mathbf{w}^3_5(z) & \mathbf{w}^3_6(z) & \mathbf{w}^3_7(z)\end{bmatrix} \\ &\quad = \begin{bmatrix}\mathbf{w}^3_0(z) & \mathbf{w}^3_1(z)\end{bmatrix} \\ &\qquad \times \begin{bmatrix} F^2_{0,0}(z) & zF^2_{4,0}(z^{-1}) & F^2_{4,0}(z) & zF^2_{0,0}(z^{-1}) \\ F^2_{4,0}(z^{-1}) & F^2_{0,0}(z) & F^2_{0,0}(z^{-1}) & F^2_{4,0}(z)\end{bmatrix}. \end{aligned} \tag{21}$$

The set of (21) shows that the single-rate calculation of the proposed CODWT is simplified to the convolutions with filters $\mathbf{F}^1_0(z)$ and filters $F^1_{0,0}(z), F^2_{0,0}(z), F^2_{4,0}(z)$ with the use of a set of lattice structures of Fig. 3. To demonstrate this in practice, based on (21), Fig. 4(a) shows the calculation of the ODWT subbands of level 3 under the single-rate construction for resolution scalability. In the figure, a set of three processor elements (PEs) is used for the production of subbands $\mathbf{w}^3_i, 1 \le i < 8$. The definition of a PE is given in Fig. 4(b); it contains four lattice structures such as the one shown in Fig. 3. In the general case of decomposition level k, the calculation structure of Fig. 4(a) uses $2^{k-1}-1$ PEs for the production of the $\mathbf{w}^k_{\mathrm{ODWT}}$ subbands.

3) Calculation of the Multirate Part of the Proposed CODWT: Concerning the multirate part of the $\mathbf{w}^k_{\mathrm{ODWT}}$ given in (16), for each level k, the calculation of the single-rate part is augmented by each of the terms $\boldsymbol{\mathcal{L}}^l_p(\mathbf{F}^l_d(z)\mathbf{d}^{k-1,l}(z)), 0 \le l < k$. The explicit form of these terms was given in (17); it consists of the convolutions $F^{l-i+1}_{w(i)+1}(z)D^{k-i}(z), 1 \le i \le l$, i.e., the elements of $\mathbf{F}^l_d(z)$ and $\mathbf{d}^{k-1,l}(z)$ followed by filtering-and-downsampling with the analysis filterbank. Fig. 5 presents an efficient calculation structure for the multirate part of (16) for $k = 3$. In the figure, the recursive definition of filters $F^{l-i+1}_{w(i)+1}(z)$ given by (9) and the symmetry property of (20) are used for the reduction of the necessary multiplications. Specifically, the lattice structure of Fig. 3 is used for the production of the results of the convolutions with filters $F^2_1(z), F^2_5(z)$. In general, the figure demonstrates that a recursive calculation is used: For each subband $D^l_0(z), 1 \le l < k$, a new stage is inserted with filter $F^1_1(z)$ and $2^{l-1}-1$ lattice structures (see the left side of the figure); also, $2^l - 2$ lowpass

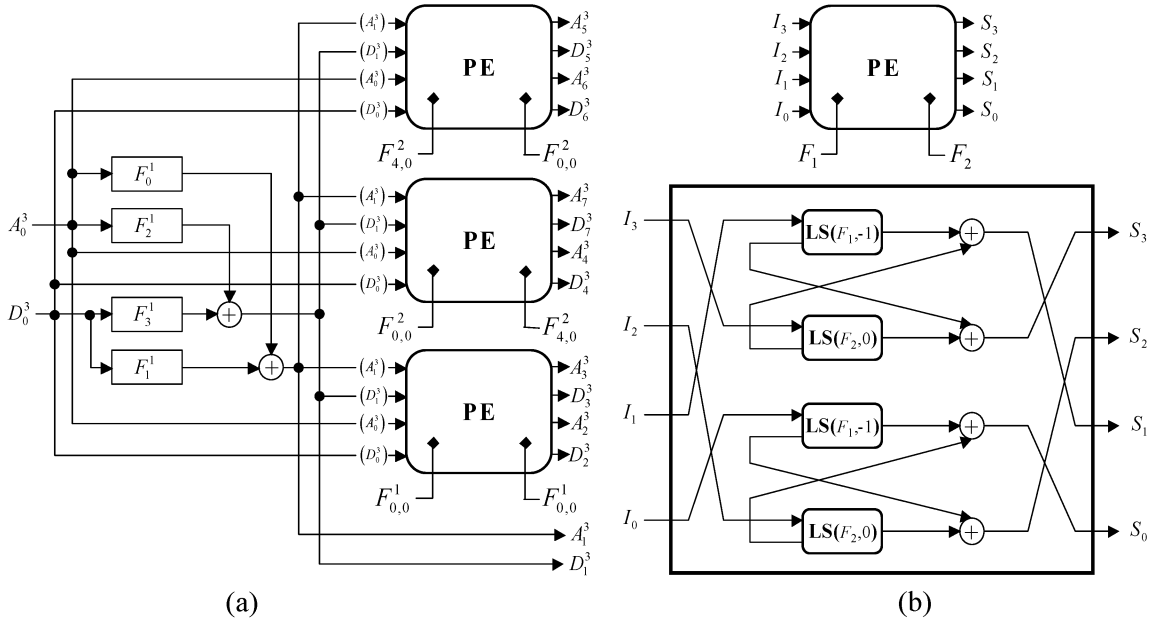

Fig. 4. (a) Calculation of the single-rate part of (16). An example with $k = 3$ is given, where the ODWT is computed using subbands A_0^3, D_0^3, and three processing elements (PEs). (b) Design of a PE.

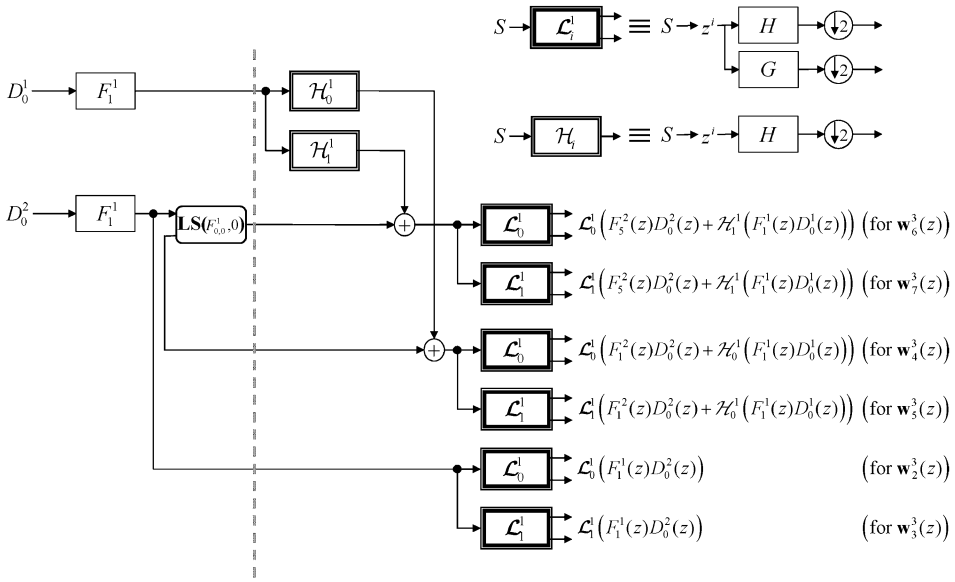

Fig. 5. Calculation of the multirate part of (16). An example with $k = 3$ is given.

filtering-and-downsampling operations are applied to subband $D_0^{l-1}(z), 1 < l < k$. In addition, $2^k - 2$ analysis filterbanks are used for $D_0^{k-1}(z)$.

IV. Computational Benefits of the Proposed CODWT in Applications

We evaluate the computational requirements of the proposed CODWT (Proposition 3) versus the conventional approach that uses the IDWT and LBS algorithm for the production of the $\mathbf{w}_{\mathrm{ODWT}}^k(z)$ subbands. In addition to that, by focusing on practical applications [4]–[17], we examine the computational complexity and delay for the transform part of a system that encodes/decodes using the CODWT in a resolution-scalable framework. In this paper, the computational complexity is formulated based on the number of required multiplications and additions. Furthermore, for a coding system that utilizes the CODWT of k levels, we define the delay for the transform part that produces the ODWT of level $l, 1 \leq l \leq k$ as the total time (in processing cycles) that is required to produce the ODWT of that resolution level.

A. Computational Complexity for the Calculation of the $\mathbf{w}_{\mathrm{ODWT}}^k(z)$ Subbands

For a one-level critically sampled wavelet decomposition or reconstruction of an N-sample signal, the computational complexity can be expressed as

$$\mathrm{DWT}(N) = \left(\frac{N}{2} I_{\mathrm{mult}}\right) \mathrm{Cost}_{\mathrm{mult}} + \left(\frac{N}{2} I_{\mathrm{add}}\right) \mathrm{Cost}_{\mathrm{add}} \tag{22}$$

where $\text{Cost}_{\text{mult}}$ and Cost_{add} express the implementation complexity of one multiplication and addition, respectively, and I_{mult} and I_{add} are factors that denote the number of multiplications and additions for each application of the filterbank to the input. For a decomposition where only the low- or the high-frequency subband is produced, these factors are replaced in (22) by $\text{f}_{U,\text{mult}}$ and $\text{f}_{U,\text{add}}$, which denote the computations (multiplications and additions) performed by one application of each filter $U = \{H, G\}$. All these factors depend on the implementation (e.g., convolution-based or lifting-based [25]). For example, by using the classical lifting factorization proposed in [20] and [25] for the 9/7 filter-pair, we have $\text{I}_{\text{mult}} = 4$ and $\text{I}_{\text{add}} = 8$, instead of $\text{I}_{\text{mult}} = 9$ and $\text{I}_{\text{add}} = 14$ achieved with convolution.[1]

As explained in Section II-B, the conventional multirate approach for the production of subbands $\mathbf{w}^k_{\text{ODWT}}(z)$ consists of the inverse DWT followed by the LBS algorithm. For a k-level DWT decomposition, after a few straightforward summations of terms $\text{DWT}(N/2^l), 0 \le l < k$, the complexity of the construction in the FO mode (production of w^k_{ODWT}) is

$$\begin{aligned}\text{LBS}(k) &= N[\text{I}_{\text{mult}}(2-2^{1-k})+\text{f}_{H,\text{mult}}(k-2+2^{1-k})]\text{Cost}_{\text{mult}} \\ &+ N[\text{I}_{\text{add}}(2-2^{1-k})+\text{f}_{H,\text{add}}(k-2+2^{1-k})]\text{Cost}_{\text{add}} \quad (23)\end{aligned}$$

where $\text{LBS}(k)$ denotes the computational complexity of the conventional approach.

Concerning the proposed approach, as explained in Section III-B2, Fig. 4(a) demonstrates the calculation of the single-rate part of (16). For each processor element (PE) of Fig. 4(a), if the applied filters F_1, F_2 have T_{F_1}, T_{F_2} nonzero coefficients, respectively, $2(T_{F_1} + T_{F_2})$ multiplications and $4(T_{F_1} + T_{F_2}) - 4$ additions are performed within the PE for each set of four inputs; notice that this holds for $k > 1$, and as for $k = 1$, there are no PEs. Using Fig. 4, the computational complexity of the single-rate part of the proposed CODWT in FO construction mode can be deduced:

$$\begin{aligned}\text{PF}_{\text{SR}}(k) = \frac{N}{2^k}\Bigg[&\left\lfloor\frac{T_{F_0^1}+1}{2}\right\rfloor + T_{F_1^1} + T_{F_2^1} + \left\lfloor\frac{T_{F_3^1}+1}{2}\right\rfloor \\ &+ 2\sum_{l=2}^{k}\sum_{i=0}^{2^{l-2}-1}\left(T_{F^{l-1}_{4i,0}} + T_{F^{l-1}_{2^l-4-4i,0}}\right)\Bigg]\text{Cost}_{\text{mult}} \\ &+ \frac{N}{2^k}\Bigg[\sum_{i=0}^{3}\left(T_{F_i^1}-1\right)+2 \\ &+ 4\sum_{l=2}^{k}\sum_{i=0}^{2^{l-2}-1}\left(T_{F^{l-1}_{4i,0}} + T_{F^{l-1}_{2^l-4-4i,0}} - 2\right) \\ &+ 4(2^{k-1}-1)\Bigg]\text{Cost}_{\text{add}} \quad (24)\end{aligned}$$

where $\text{PF}_{\text{SR}}(k)$ is the computational complexity[2] of the single-rate part of (16) for the production of w^k_{ODWT}, and $T_{F_i^l}$ is the number of nonzero coefficients of filter F_i^l.

From the description of Section III-B3 and Fig. 5, the computational complexity of the multirate part of (16) for the general case of k decomposition levels can be deduced. Specifically, for each subband $D_0^l(z), 1 \le l < k$

$$\begin{aligned}&\text{PF}_{\text{MR}}(k) \\ &= N\Bigg[\sum_{l=1}^{k-1}\Big(2^{-l}\Big(T_{F_1^1} + \text{f}_{\text{LS,mult}}(l) + \text{f}_{\text{an}}(l)\text{f}_{H,\text{mult}}\Big)\Big) \\ &\quad + 2^{-k}\text{f}_{\text{an}}(k)\text{I}_{\text{mult}}\Bigg]\text{Cost}_{\text{mult}} \\ &\quad + N\Bigg[\sum_{l=1}^{k-1}\Big(2^{-l}\Big(T_{F_1^1} - 1 + \text{f}_{\text{LS,add}}(l) \\ &\quad + \text{f}_{\text{an}}(l)(\text{f}_{H,\text{add}}+1)\Big)\Big) + 2^{-k}\text{f}_{\text{an}}(k)\text{I}_{\text{add}}\Bigg]\text{Cost}_{\text{add}}\end{aligned} \quad (25)$$

where, for each subband $D_0^l(z)$, the multiplication and addition-related factors for the used lattice structures are $\text{f}_{\text{LS,mult}}(l) = \sum_{i=1}^{l-1}\sum_{j=0}^{2^{i-1}-1} T_{F^i_{4j,0}}, \text{f}_{\text{LS,add}}(l) = 2\sum_{i=1}^{l-1}\sum_{j=0}^{2^{i-1}-1}(T_{F^i_{4j,0}} - 1)$ for $l > 1$, where $\text{f}_{\text{LS,mult}}(1) = 0, f_{\text{LS,add}}(1) = 0$. In addition, $\text{f}_{\text{an}}(l) = 2^l - 2$ is the number of the used lowpass filters.

Note that as shown in (16), the multirate calculation occurs for $k > 1$. For this case, the total complexity of the final result of (16) is given by

$$\text{PF}(k) = \text{PF}_{\text{SR}}(k) + \text{PF}_{\text{MR}}(k) + N(2-2^{1-k})\text{Cost}_{\text{add}}. \quad (26)$$

The last term of (26) corresponds to the complexity of the additions between the single- and multirate part of the transform in order to create the final result.

It is important to notice that the results of this section are applicable also for the 2-D case of a $C \times R$ input image since both techniques can be applied in a separable manner along the rows and columns of the input. Specifically, the 2-D implementation of the proposed CODWT for any level k consists of 1) applying the prediction-filters row-wise to the 2-D DWT subbands using the calculation scheme of Figs. 4(a) and 5, thereby producing the ODWT subbands with phase $(0, i), 1 \le i < 2^k$ (2-D phase [5], [9]); and 2) the column-wise filtering of the resulting subbands with the same 1-D scheme. Hence, to produce the $2^k \times 2^k$ ODWT subbands of level k, the complexity associated with the row-wise filtering is $(R/2^k) \times \text{PF}(k)$. In addition, the complexity of the column-wise filtering is $C \times \text{PF}(k)$. In the same manner, the separable application of the 1-D LBS approach indicates that the complexity is $(R/2^k + C) \times \text{LBS}(k)$. As a result, the complexity reduction offered by the proposed approach is $1 - (\text{PF}(k))/(\text{LBS}(k))$ in both the 1-D and 2-D cases.

[1]Note that we will estimate the complexity of lifting factorizations without scaling factors in order to minimize the arithmetic complexity. In a coding system, the multiplications with these factors can be implicitly performed by embedding the scaling factors in the quantization formulas applied to each subband at each resolution level.

[2]In (24), the number of multiplications for the prediction filters of level 1 is reduced by taking advantage of the symmetry property of (19), which also holds for filter $F_3^1(z)$ since $F_0^1(z) = -F_3^1(z)$ from the definitions of (4). Furthermore, if one restricts the complexity analysis to biorthogonal filter pairs, it is straightforward to prove that $F_1^1(z^{-1}) = F_1^1(z), F_2^1(z^{-1}) = z^{-2}F_2^1(z)$ and use these symmetries to further reduce the multiplications reported in (24).

TABLE I
MULTIPLICATIONS AND ADDITIONS FOR THE CODWT OF VARIOUS LEVELS, NORMALIZED PER INPUT SAMPLE

9/7 filter-bank [20] [25]			$I_{multiply}=9, I_{add}=14$	
Construction of decomposition level *k*:	**Proposed (Mpp)**	**IDWT+ LBS (Mpp)**	**Proposed (App)**	**IDWT+ LBS (App)**
1	8.5	9	15	14
2	15.25	16	27	25
3	23.625	22	40.5	34.5
7/5 filter-bank [21] [22]			$I_{multiply}=7, I_{add}=10$	
1	6.5	7	11	10
2	11.75	12.5	20	18
3	18.125	17.25	29.5	25
4/4 filter-bank [25]			$I_{multiply}=4, I_{add}=6$	
1	6	4	7	6
2	11.5	8	14.25	10.5
3	18.75	12	21.25	14.25

Mpp: Multiplications per pixel (average), App: Additions per pixel (average)

For a numerical comparison between the two approaches, by using (26) for the proposed CODWT and (23) for the conventional IDWT+LBS approach, we identified that both methods have comparable arithmetic complexity under a convolution-based implementation. This is shown in Table I, where numerical examples of the multiplication and addition requirements are presented for the levels $k = 1, 2, 3$ using the proposed and the conventional approaches. Both cases have been normalized by the number of input samples (pixels) N. The use of lifting reduces the computational requirements for both approaches; however, we generally found that lifting factorizations tend to benefit less the proposed approach since they are only used in the analysis filters of the multirate part of the transform.

On the other hand, as shown in Table II, the proposed approach exhibits a *practical* reduction in computation times in comparison to the conventional method for "ANSI-C" implementations running on a personal computer with an Intel Pentium IV processor. Both convolution-based and lifting-based implementations have been tested. The experiments were carried out for an SD-resolution video sequence (720×480 pixels, three color channels, 100 frames) with the 9/7 filter pair. The row-column implementation was used for both methods. Table II demonstrates that the proposed approach runs, on average, 35.83% faster in comparison to the conventional approach when both employ a lifting-based implementation. Profiling of the execution revealed that, although the proposed method performs (on average) more instruction-related operations in the case of lifting-based implementations, a significantly better utilization of the cache memory is achieved in comparison to the IDWT + LBS approach. This is attributed to the fact that by using the proposed calculation scheme, the proposed CODWT utilizes the same input to produce a number of intermediate results; for example, Fig. 4(a) demonstrates that the single-rate part of all the subbands of level 3 is produced by using $A_0^3(z), D_0^3(z), A_1^3(z), D_1^3(z)$. As a result, the proposed CODWT achieves a significantly higher locality in the processing. This leads to the speedup in computation times reported in Table II.

In resolution-scalable coding, the comparison between the lifting-based implementations of the proposed CODWT and LL-LBS approaches is given in Table III. The case of a coding system that supports a maximum of $k = 4$ decomposition (resolution) levels and decodes to any output resolution-level $l, 1 \leq l \leq k$ is assumed. In this scenario, as explained in Section II-B, decoding a resolution level l requires that the CODWT is performed for resolution levels $k, k-1, \ldots, l$. These results show that in resolution-scalable coding, the proposed CODWT achieves notable complexity reductions in comparison to LL-LBS. Furthermore, we find that significant reductions in the computation time are experimentally observed. This is shown in Table IV, where we assume a resolution-scalable scenario with a HDTV video sequence processed in four (dyadically reduced) resolutions, ranging from 1920×1088 pixels ($l = 1$) to 240×136 pixels ($l = 4$). The proposed CODWT exhibits an average reduction of 78.45% in computation time for lifting implementations.

TABLE II
PERCENTAGE OF SPEEDUP IN EXECUTION TIME OF THE PROPOSED METHOD VERSUS THE CONVENTIONAL APPROACH (9/7 FILTER-BANK) IN A PENTIUM IV PROCESSOR

Construction of decomposition level *k*:	**Convolution based** Speedup of proposed vs LBS	**Lifting based** Speedup of proposed vs LBS
1	77.12 %	69.02 %
2	38.54 %	33.31 %
3	12.43 %	5.15 %
Average:	42.70 %	35.83 %

An interesting observation stemming from Table III is that the computational complexity of both techniques scales up with the number of decoded resolution levels: a result that is highly useful for complexity-scalable image and video coding.

The significant complexity reductions of Tables III and IV that are achieved with the proposed approach in resolution scalable scenarios can be attributed to the following two aspects.

- A single-rate calculation is used. Hence, the series of inverse and forward wavelet transforms required by the conventional multi-rate approach is avoided.
- The scheme of Section III-B2 reduces the complexity based on the filter symmetries of (20).

TABLE III
MULTIPLICATION AND ADDITION BUDGET FOR THE CODWT IN A RESOLUTION-SCALABLE CODEC WITH FOUR DECOMPOSITION LEVELS. THREE REPRESENTATIVE FILTERBANKS (OF VARYING COMPLEXITY) USED IN LOSSY IMAGE AND VIDEO CODING ARE PRESENTED

CODWT stops at level l:	Multiplications		Reduction (%)	Additions		Reduction (%)
	Proposed (Mpp)	LL-LBS (Mpp)		Proposed (App)	LL-LBS (App)	
9/7 filter-bank, ($\mathrm{I}_{\mathrm{mult}} = 4,\ \mathrm{I}_{\mathrm{add}} = 8$) [20] [25, Section 7.7]						
1	23.8125	35.75	**33.39**	52.75	71.5	**26.22**
2	19.8125	32.25	**38.57**	38.25	64.5	**40.70**
3	15.8125	25.5	**37.99**	27.5	51	**46.08**
4	11.0625	15.125	**26.86**	17.625	30.25	**41.74**
7/5 filter-bank, ($\mathrm{I}_{\mathrm{mult}} = 3,\ \mathrm{I}_{\mathrm{add}} = 6$) [21] [22, Table 2]						
1	17.8125	25.75	**30.83**	37.25	51.50	**27.67**
2	14.8125	23.25	**36.29**	26.75	46.5	**42.47**
3	11.8125	18.5	**36.15**	19	37	**48.65**
4	8.3125	11.125	**25.28**	12.125	22.25	**45.51**
4/4 filter-bank, ($\mathrm{I}_{\mathrm{mult}} = 2,\ \mathrm{I}_{\mathrm{add}} = 5$) [25, Section 7.5]						
1	13.25	30	**55.83**	20.75	33.75	**38.52**
2	10.25	27	**62.04**	14.25	29.75	**52.10**
3	7.75	21	**63.10**	9.5	23.25	**59.14**
4	5.25	12	**56.25**	5.625	14	**59.82**

Mpp: Multiplications per pixel (average), App: Additions per pixel (average)

TABLE IV
EXAMPLE OF SPEEDUP IN COMPUTATION TIMES FOR THE CODWT UNDER RESOLUTION-SCALABLE CONSTRUCTION; ONE HUNDRED FRAMES OF A HDTV COLOR VIDEO SEQUENCE (1920 × 1088 PIXELS) WERE USED WITH THE 9/7 FILTERBANK

CODWT stops at level l:	Speedup of proposed vs. LL-LBS using convolution	Speedup of proposed vs. LL-LBS using lifting
1	82.33 %	77.78 %
2	82.58 %	78.20 %
3	84.95 %	81.08 %
4	82.00 %	76.75 %
Average:	82.96 %	78.45 %

As a result, the proposed approach becomes *increasingly* more efficient in comparison to the conventional approach as the resolution-level l increases. Interestingly, this tendency is reversed at the coarsest resolution level where the computational-reduction percentage offered by the proposed approach is usually decreased (see Table III and experimental results of Table IV). This phenomenon occurs since the ODWT of the coarsest resolution is constructed in FO mode (i.e., both the low- and high-frequency ODWT subbands are created), whereas the ODWT of the lower resolution levels are constructed in HFO-mode (i.e., only the high-frequency ODWT subbands are created).

B. Delay for the Level-by-Level Calculation of the $\mathbf{w}^k_{\mathrm{ODWT}}(z)$ Subbands

Assuming the classical point-symmetric or periodic extension for the signal edges, consider that the two methods are implemented in a system where one application of a filter (or filter-bank) on a set of input samples requires a_{LBS} processing cycles for the LL-LBS method and a_{PF} processing cycles for the prediction-filters method. To diminish the side effects of scheduling algorithms for the multiple filtering operations, we assume the case of high parallelism, where one filter per required convolution is present (similar to the system of [24]). In this way, every filtering application initiates as soon as sufficient input is present [24]. Furthermore, to facilitate the description, the delay resulting from the storage or retrieval of intermediate results is not taken into account.

Starting with the LL-LBS method, k single-level inverse transforms and $\sum_{l=1}^{k}(2^l - 1)$ single-level forward transforms are performed for the production of the subbands of the ODWT of level k; see the example in Fig. 1(b) for $k = 3$. After an initiation latency (which is denoted $L_{\mathrm{init,LL-LBS}}(k)$), the first coefficients of the reconstructed input signal $\overline{X}$ are produced. Then, all filter kernels of every level work in parallel to perform the inverse and forward transforms. This is equivalent to a cascade connection of the inverse and forward recursive pyramid algorithm of Vishwanath [24].

The total time required for the completion of the calculation of all subbands is determined by the delay for the production of the signal with the maximum length, since during this

TABLE V
EXAMPLES OF THE ODWT DELAY-REDUCTION GAINS OFFERED BY THE PROPOSED APPROACH (FO-MODE, 9/7 FILTER-PAIR) FOR VARIOUS DECOMPOSITION LEVELS OF A 512-SAMPLE SIGNAL. THREE INDICATIVE CASES FOR THE RATIO $u_c = a_{\mathrm{LBS}}/a_{\mathrm{PF}}$ ARE USED

Level k	$\frac{L_{\mathrm{LL-LBS}}(k,512)}{L_{\mathrm{PF}}(k,512)}$ **with** $u_c = 0.5$	$\frac{L_{\mathrm{LL-LBS}}(k,512)}{L_{\mathrm{PF}}(k,512)}$ **with** $u_c = 1$	$\frac{L_{\mathrm{LL-LBS}}(k,512)}{L_{\mathrm{PF}}(k,512)}$ **with** $u_c = 2$
1	0.51	1.01	2.03
2	0.96	1.92	3.84
3	1.78	3.56	7.11
4	2.99	5.98	11.96

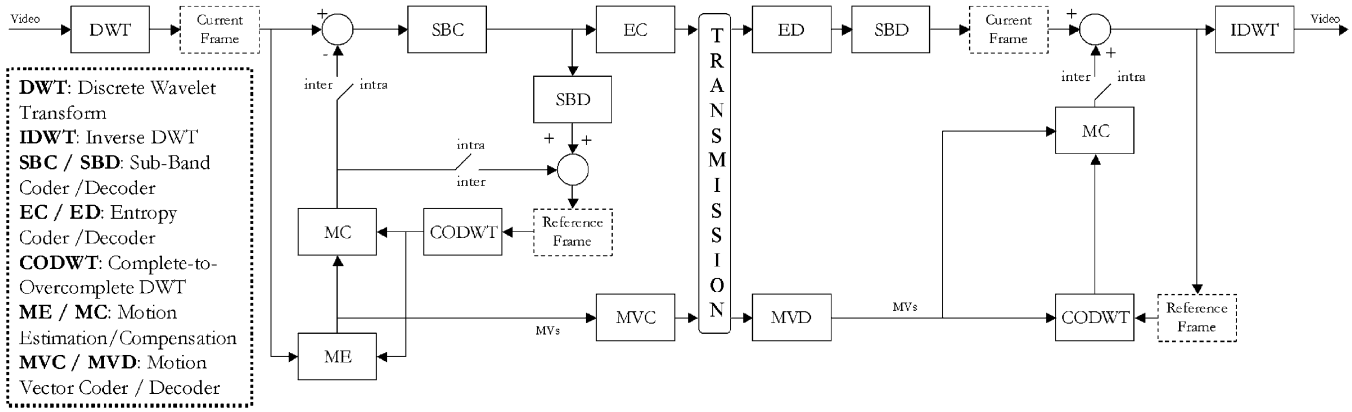

Fig. 6. Architecture of a predictive coder with wavelet-domain (in-band) ME/MC that uses the resolution-scalable CODWT.

process the highest number of *consecutive* filter applications occurs [24]. The signal with the maximum length produced by the LL-LBS is the reconstructed input signal $\bar{X}$. The production of $\bar{X}$ requires $(N/2)$ applications of filter $\tilde{H}$ (synthesis lowpass filter). Additionally, after the production of all samples of $\bar{X}$, the completion of the forward transforms at each level requires an additional number of filtering operations that will cause an additional number of processing cycles, which are denoted as $L_{\mathrm{comp,LL-LBS}}(k)$. Hence, the total delay of the LL-LBS system for the production of all the subbands of decomposition level k for an N-point input signal is

$$L_{\mathrm{LL-LBS}}(k,N) = L_{\mathrm{init,LL-LBS}}(k) + \frac{N}{2}a_{\mathrm{LBS}} + L_{\mathrm{comp,LL-LBS}}(k). \quad (27)$$

For the prediction-filters method, the application of filters $F_0^1, \ldots, F_3^1$ to A_0^k, D_0^k can be initiated in parallel for the calculation of subbands A_1^k, D_1^k. After this initiation, which in this case requires $L_{\mathrm{init,PF}}(k)$ processing cycles, the PEs that produce the rest of the subbands of level k (if $k > 1$) can also be applied in parallel by reusing the coefficients of subbands A_1^k, D_1^k, as seen in Fig. 4(a). As a result, the required delay for the completion of the process is

$$L_{\mathrm{PF}}(k,N) = L_{\mathrm{init,PF}}(k) + \frac{N}{2^k}a_{\mathrm{PF}}. \quad (28)$$

Equations (27) and (28) show that, in systems that can achieve a high-degree of hardware parallelism, the delay of the proposed CODWT for resolution level k is expected to be proportional to $(N/2^k)a_{\mathrm{PF}}$, while the LL-LBS approach achieves a delay proportional to $(N/2)a_{\mathrm{LBS}}$. Examples of the delay ratios between the two approaches under this high-parallelism scenario are given in Table V. Since it is difficult to quantify the actual ratio between the factors a_{PF} and a_{LBS} without measurements from a realization of the two approaches in a custom hardware design, we resort to reporting the delay-reduction gains offered by the proposed approach under three assumptions: $a_{\mathrm{LBS}} = u_c \cdot a_{\mathrm{PF}}$, with $u_c = \{0.5, 1, 2\}$, corresponding to a "pessimistic," "average," and "optimistic" case for the relative efficiency in hardware implementation of the proposed method versus the conventional approach.

For the 2-D processing of a $C \times R$ image, as explained before, both methods can be implemented via two identical one-dimensional (1-D) systems used row-wise and column-wise. However, instead of processing all the rows and consequently processing the columns, the filtering in each direction can be interleaved, and the column processing begins after an initiation latency so that enough coefficients exist column-wise for the mirroring and for the initiation of the filter-applications required for every method. Hence, the comparison of both methods in terms of delay for the 2-D CODWT follows the result of the 1-D case.

V. APPLICATIONS

A number of coding applications that require wavelet-domain operations in the ODWT [1]–[16] can benefit from the proposed transform formulation. In Section IV, we focused on the level-by-level CODWT, which is applied in coding schemes that target progressive-refinement in resolution [4]–[16]. Below, we briefly discuss these scalable coding applications.

Motion-compensated wavelet video coders with in-band prediction have been proposed in [1]–[3] and [5]–[9]. There, the conventional closed-loop coding schemes are modified in order to provide resolution scalability, as seen in the architecture of Fig. 6. The encoder performs motion estimation and compensation (ME/MC) in the wavelet domain (in-band) following

TABLE VI
AVERAGE PSNR (IN DECIBELS, LUMINANCE CHANNEL) FOR TWO TYPICAL SEQUENCES IN CIF RESOLUTION (PROGRESSIVELY SCANNED, 352 × 288 FRAMES/S). FOR THE COMPARISON AT HALF RESOLUTION, THE NONSCALABLE MPEG-4 AND THE CONVENTIONAL SPATIAL-DOMAIN ME/MC CODER SEPARATELY ENCODED THE LOW-FREQUENCY SUBBAND OF THE ONE-LEVEL DWT OF EACH FRAME

Sequence:	**"Stefan": CIF resolution, 300 frames**		**"Bus": CIF resolution, 150 frames**	
Bit-rate: (full-resolution)	2 Mbps	3 Mbps	2 Mbps	3 Mbps
In-band ME/MC *	**34.47**	**37.90**	**34.63**	**36.25**
Spatial-domain ME/MC	33.74	35.61	33.79	35.61
MPEG-4, non-scalable	34.29	36.86	34.53	35.92
Bit-rate: (half-resolution)	900 Kbps	1.5 Mbps	600 Kbps	1.2 Mbps
In-band ME/MC *	**33.71**	**38.72**	**31.44**	**37.48**
Spatial-domain ME/MC	33.06	36.12	30.95	36.15
MPEG-4, non-scalable	33.31	36.75	30.83	36.06

* This technique is using the CODWT and is the only one that provides the results of both resolutions with one bitstream.

a level-by-level refinement of the compressed information. However, since the critically sampled wavelet decomposition is only periodically shift-invariant, the ME/MC procedures are performed in the ODWT domain [1]–[3], which is constructed per resolution level by the CODWT module. In this way, the produced bit-stream can be decoded at a variety of resolutions without drifting problems [5]–[8], [9], [13].

In Table VI, we present typical coding results obtained with the resolution-scalable video coder of [9] equipped with half-pixel accurate in-band ME and employing a two-level decomposition $(k = 2)$ with the 9/7 filter pair. The quantization and entropy coding is performed with the QuadTree-Limited (QT-L) coder of [28], which is an intraband embedded wavelet coding algorithm combining quadtree coding and block-based coding of the significance maps [28]. Decoding to level $l = 1$ (full-resolution) and $l = 2$ (half-resolution) is performed. For comparison purposes, Table VI presents the results obtained with two *nonscalable* solutions: the equivalent coder that performs conventional spatial-domain ME/MC [1], [9] followed by DWT and error-frame coding, the nonscalable DCT-based MPEG-4 coder using half-pixel ME/MC, and the same block-size, search range, and prediction structure (I and P frames). It is important to notice that the proposed scalable system produces the two resolution levels from the same compressed bit-stream. In contrast, the two nonscalable systems generate one bit-stream per resolution and target bit-rate, with the low-resolution video produced using the uncoded low-frequency subbands of the one-level DWT as input.

The results of Table VI demonstrate that the proposed system outperforms the equivalent system using spatial-domain ME/MC and the nonscalable MPEG-4 coder, both producing *either* of the two resolution levels. Although we present PSNR for the luminance channel only, similar gains occur for the chrominance channels as well. In a video broadcasting scenario, the nonscalable codecs require, for example, 2.9 Mb/s to provide two resolutions of the "Stefan" sequence (see Table VI), while the proposed system provides both resolutions with superior PSNR quality at only 2 Mb/s.

Alternative systems for scalable video coding are the open-loop video coding algorithms proposed in [10]–[15], employing wavelet-domain motion estimation and motion-compensated temporal filtering (MCTF) [29], [30]. The conventional approaches for open-loop video coding apply MCTF on the input frames and perform DWT on the resulting motion-compensated residual frames [29]. In contrast to these techniques, the in-band MCTF systems of [10]–[15] first decompose spatially the video frames into multiple subbands using the DWT and then remove the temporal correlations for each subband using MCTF in the wavelet domain. The residual signal after the MCTF can be coded using any desired texture-coding technique (DCT-based, wavelet-based, matching pursuit, etc.). In this way, decoding to arbitrary resolution, quality, or frame rate is achieved from a single compressed bit stream. In these systems, for efficient wavelet-domain ME, the ODWT can be constructed from the critically sampled DWT of the reference frames, assuming resolution scalability. In [11]–[13], a comparison of the coding efficiency of spatial-domain and in-band MCTF employing the level-by-level CODWT is performed under many different scenarios. The results demonstrated that the in-band MCTF system achieves comparable or superior coding efficiency in comparison to the spatial-domain alternative for the vast majority of the tests [11]–[15].

Another application that uses the CODWT is the still-image coding system proposed in [16]. In that system, the level-by-level CODWT is used for the realization of a scheme that performs phase-based prediction of the subbands of each resolution level. Hence, instead of simply coding, with an intra-band coder, the original subband content, a prediction of the subband coefficients of each resolution level is performed using the interpolated ODWT of the previous-level subbands, which, in a resolution-scalable framework, can be constructed independently at both the encoder and decoder sides using the CODWT. Significant coding gains are reported in comparison to the codec using the same subband and entropy-coding techniques and no ODWT-based prediction [16].

VI. CONCLUSION

A new framework is presented for the construction of the overcomplete DWT starting from the subbands of the critically sampled decomposition. The proposed framework has inherent advantages, in comparison to the conventional approach, since it

consists of a direct transform from the complete to the overcomplete DWT, using the minimum number of downsampling operations and no upsampling. For image and video coding applications that utilize a level-by-level construction of the ODWT, it is demonstrated that the proposed CODWT has significant implementation advantages over the conventional approach because it offers a) significant computation savings and b) a single-rate calculation that can provide a scalable reduction in the transform-production delay. These features lead to inherent computational scalability in comparison to the conventional approach. Finally, concrete application examples that use the proposed transform have been presented.

REFERENCES

[1] H. W. Park and H. S. Kim, "Motion estimation using low-band-shift method for wavelet-based moving-picture coding," *IEEE Trans. Image Process.*, vol. 9, no. 4, pp. 577–587, Apr. 2000.

[2] J. Skowronski, "Pel recursive motion estimation and compensation in subbands," *Signal Process.: Image Commun.*, vol. 14, no. 5, pp. 389–396, Apr. 1999.

[3] R. Zaciu, C. Lamba, C. Burlacu, and G. Nicula, "Image compression using an overcomplete discrete wavelet transform," *IEEE Trans. Consum. Electron.*, vol. 42, no. 3, pp. 800–807, Aug. 1996.

[4] G. Van der Auwera, A. Munteanu, P. Schelkens, and J. Cornelis, "Bottom-up motion compensated prediction in the wavelet domain for spatially scalable video," *Electron. Lett.*, vol. 38, no. 21, pp. 1251–1253, Oct. 2002.

[5] X. Li, L. Kerofski, and S. Lei, "All-phase motion compensated prediction in the wavelet domain for high performance video coding," in *Proc. IEEE Int. Conf. Image Process.*, vol. 3, Thessaloniki, Greece, Oct. 2001, pp. 538–541.

[6] X. Li and L. Kerofsky, "High performance resolution scalable video coding via all-phase motion-compensated prediction of wavelet coefficients," in *Proc. SPIE Visual Commun. Image Process.*, San Jose, CA, Jan. 2002, pp. 1080–1090.

[7] C. Mayer, "Motion compensated in-band prediction for wavelet-based spatially scalable video coding," in *Proc. IEEE Int. Conf. Acoust., Speech, Signal Process.*, vol. 3, Hong Kong, Apr. 2003, pp. 73–76.

[8] C. Mayer and S. Albert, "Scalable video coding with in-band prediction," in *Proc. SPIE Elec. Imaging—Image Video Commun. Process.*, vol. 5022, Santa Clara, CA, May 2003, pp. 973–983.

[9] Y. Andreopoulos, A. Munteanu, G. Van der Auwera, P. Schelkens, and J. Cornelis, "Scalable wavelet video-coding with in-band prediction—Implementation and experimental results," in *Proc. IEEE Int. Conf. Image Process.*, vol. 3, Rochester, NY, Sep. 2002, pp. 729–732.

[10] Y. Wang, S. Cui, and E. Fowler, "Fully scalable video coding using redundant-wavelet multihypothesis and motion-compensated temporal filtering," in *Proc. IEEE Int. Conf. Image Process.*, vol. 2, Barcelona, Spain, Sep. 2003, pp. 53–56.

[11] Y. Andreopoulos, M. van der Schaar, A. Munteanu, J. Barbarien, P. Schelkens, and J. Cornelis, "Fully scalable wavelet video coding using in-band motion compensated temporal filtering," in *Proc. IEEE Int. Conf. Acoust., Speech, Signal Process.*, vol. 2, Hong Kong, Apr. 2003, pp. 795–798.

[12] ——, "Open-loop, in-band motion-compensated temporal filtering for objective full-scalability in wavelet video coding," in *ISO/IEC JTC1/SC29/WG11, m9026, MPEG*, Shanghai, China, Oct. 2002.

[13] Y. Andreopoulos, A. Munteanu, J. Barbarien, M. Van der Schaar, J. Cornelis, and P. Schelkens, "In-band motion compensated temporal filtering," *Signal Process.: Image Commun. Special Issue Interframe Wavelet Video Coding*, to be published.

[14] J. Ye and M. van der Schaar, "3-D lifting structure for sub-pixel accuracy motion compensated temporal filtering in overcomplete wavelet domain," in *ISO/IEC JTC1/SC29/WG11, m9554, MPEG*. Pattaya, Thailand, Mar. 2003.

[15] M. van der Schaar, J. Ye, Y. Andreopoulos, and A. Munteanu, "Fully scalable 3-D overcomplete wavelet video coding using adaptive motion compensated temporal filtering," in *ISO/IEC JTC1/SC29/WG11, m9037, MPEG*, Shanghai, China, Oct. 2002.

[16] X. Li, "On exploiting geometric constraint of image wavelet coefficients," *IEEE Trans. Image Process.*, vol. 12, no. 11, pp. 1378–1387, Nov. 2003.

[17] Y. Andreopoulos, A. Munteanu, G. Van der Auwera, P. Schelkens, and J. Cornelis, "A new method for complete-to-overcomplete discrete wavelet transforms," in *Proc. Int. Conf. Digit. Signal Process.*, Santorini, GR, Jul. 2002, pp. 501–504.

[18] X. Li, "New results of phase shifting in the wavelet space," *IEEE Signal Process. Lett.*, vol. 10, no. 7, pp. 193–195, July 2003.

[19] S. Mallat, *A Wavelet Tour of Signal Process.*. San Diego, CA: Academic, 1998.

[20] "JPEG 2000 part I final draft international standard," in *ISO/IEC JTC1/SC29/WG1, FCD 15444-1*, M. Boliek, C. Christopoulos, and E. Majani, Eds., Dec. 2000.

[21] "JPEG-2000 part II final committee draft," in *ISO/IEC JTC1/SC29/WG1, FCD 15444-2*, M. Boliek, Ed., Dec. 2000.

[22] C. Brislawn, "Interim report on (part 2) core experiment CodEff07, 7-tap/5-tap filter bank option," in *ISO/IEC JTC1/SC29/WG1, N1761, JPEG*, Jul. 2000.

[23] H. Sari-Sarraf and D. Brzakovic, "A shift-invariant discrete wavelet transform," *IEEE Trans. Signal Process.*, vol. 45, no. 10, pp. 2621–2626, Oct. 1997.

[24] M. Vishwanath, "The recursive pyramid algorithm for the discrete wavelet transform," *IEEE Trans. Signal Process.*, vol. 42, no. 3, pp. 673–676, Mar. 1994.

[25] I. Daubechies and W. Sweldens, "Factoring wavelet transforms into lifting steps," *J. Fourier Anal. Appl.*, vol. 4, no. 3, pp. 247–269, Mar. 1998.

[26] R. R. Coifman and D. L. Donoho, "Translation invariant de-noising," in *Wavelets and Statistics, Lecture Notes in Statistics 103*, A. Antoniadis and G. Oppenheim, Eds. New York, NY: Springer-Verlag, pp. 125–150.

[27] H. M. Radha, M. van der Schaar, and Y. Chen, "The MPEG-4 fine-grained scalable video coding method for multimedia streaming over IP," *IEEE Trans. Multimedia*, vol. 3, no. 1, pp. 53–68, Mar. 2001.

[28] P. Schelkens, A. Munteanu, J. Barbarien, M. Galca, X. Giro-Nieto, and J. Cornelis, "Wavelet coding of volumetric medical datasets," *IEEE Trans. Med. Imag. Special Issue on Wavelets in Medical Imaging*, vol. 22, no. 3, pp. 441–458, Mar. 2003.

[29] J. R. Ohm, "Three-dimensional subband coding with motion compensation," *IEEE Trans. Image Process.*, vol. 3, no. 5, pp. 559–571, Sep. 1994.

[30] D. Turaga and M. van der Schaar, "Wavelet coding for video streaming using new unconstrained motion compensated temporal filtering," in *Proc. Int. Workshop Dig. Commun. Adv. Methods for Multimedia Signal Process.*, Capri, Italy, Sep. 2002, pp. 41–48.

Yiannis Andreopoulos (S'01) was born in 1977 in Aeghion, Greece. He received the electrical engineering diploma and the M.Sc. degree in signal and image processing systems from the University of Patras, Patrtas, Greece. Since October 2000, he has been working toward the Ph.D. degree at the Vrije Universiteit Brussel (Free University of Brussels), Belgium.

His research interests are in the fields of transforms, fast algorithms, and video coding, specializing in combined algorithmic and implementation topics for hardware and software systems. He contributes regularly to the ISO/IEC JTC1/SC29/WG11 (MPEG) committee (Scalable Video Coding group).

Adrian Munteanu was born in Constanta, Romania, in 1970. He received the M.Sc. degree in electronics and telecommunications from the "Politehnica" University of Bucharest, Bucharest, Romania, in 1994, the M.Sc. degree in biomedical engineering from the Technical University of Patras, Patras, Greece, in 1996, and the Ph.D. degree in applied sciences from the Vrije Universiteit Brussel (VUB), Brussels, Belgium, in 2003.

Since October 1996, he has been a member of the Department of Electronics and Information Processing (ETRO), VUB, and since July 2003, he has been a post-doctoral researcher at ETRO. His research interests include scalable still image and video coding, multiresolution image analysis, image and video transmission over networks, video segmentation and indexing, and statistical modeling of images. He is the author or co-author of more than 70 scientific publications, patent applications, and contributions to standards, and he has contributed to two books in his areas of interest.

Geert Van der Auwera was born in Bonheiden, Belgium, in 1974. He received the electrotechnical civil engineering degree from Vrije Universiteit Brussel (VUB), Brussels, Belgium in 1997.

Presently, he is scientific advisor for IWT-Flanders, the Institute for the Promotion of Innovation by Science and Technology in Flanders, Belgium. In 2000, he joined IWT-Flanders after performing research funded by an IWT-Flanders grant at the Electronics and Information Processing Department (ETRO), VUB. His fields of interest are image and video coding and image processing.

Mr. Van der Auwera's master's thesis received the Barco and IBM prizes by the Fund for Scientific Research—Flanders.

Jan P. H. Cornelis (M'80) was born in Wilrijk, Belgium, in 1950. He received the M.D. degree in 1973 and the Ph.D. degree in 1980.

He is a professor in electronics, medical imaging, and digital image processing at the Vrije Universiteit Brussel (VUB), Brussels, Belgium, where he is also Vice-rector Research. He is director of the Electronics and Information Processing Department (ETRO), VUB, at the Faculty of Applied Sciences and coordinates the research group on image processing and machine vision (IRIS). His current research projects within the IRIS group include:various applications in medical vision, remote sensing, mine and minefield detection, and design of algorithms and computer architectures for image processing. His current research interest is mainly concentrated in the area of image and video compression.

Peter Schelkens (M'99) received the electrical engineering degree in applied physics in 1994, the Medical Physicist degree in 1995, and the Ph.D. degree in applied sciences in 2001, all from the Vrije Universiteit Brussel (VUB), Brussels, Belgium.

Since October 1994, he has been a member of the IMEC-ETRO Laboratory at the VUB, where he had a position as assistant to Prof. J. Cornelis. Since 2000, he has been leading a research team in the field of image and video compression and related multimedia technologies. The team's research focus is both on algorithmic and implementation aspects. The team is very involved in the ISO/IEC JTC1/SC29/WG1 (JPEG2000) and WG11 (MPEG) committees. He is also the Belgian head of delegation for the ISO/IEC JPEG standardization committee, and co-editor of part 10 of JPEG2000: "Extensions for Three-Dimensional and Floating Point Data."